

Mercury Neutronics Modeling of NIF Target Geometries

Presented to HEDP Intern Group
6 August 2013

Timothy Collart

Mentors – Patrick Brantley, Charlie Cerjan,
Scott McKinley, Scott Sepke



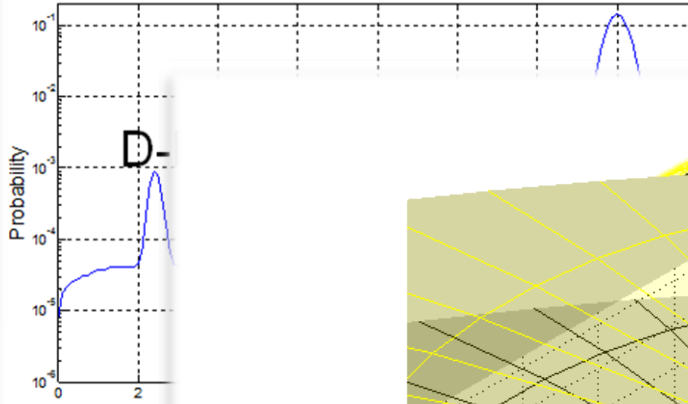
Lawrence Livermore
National Laboratory

LLNL-PRES-642312

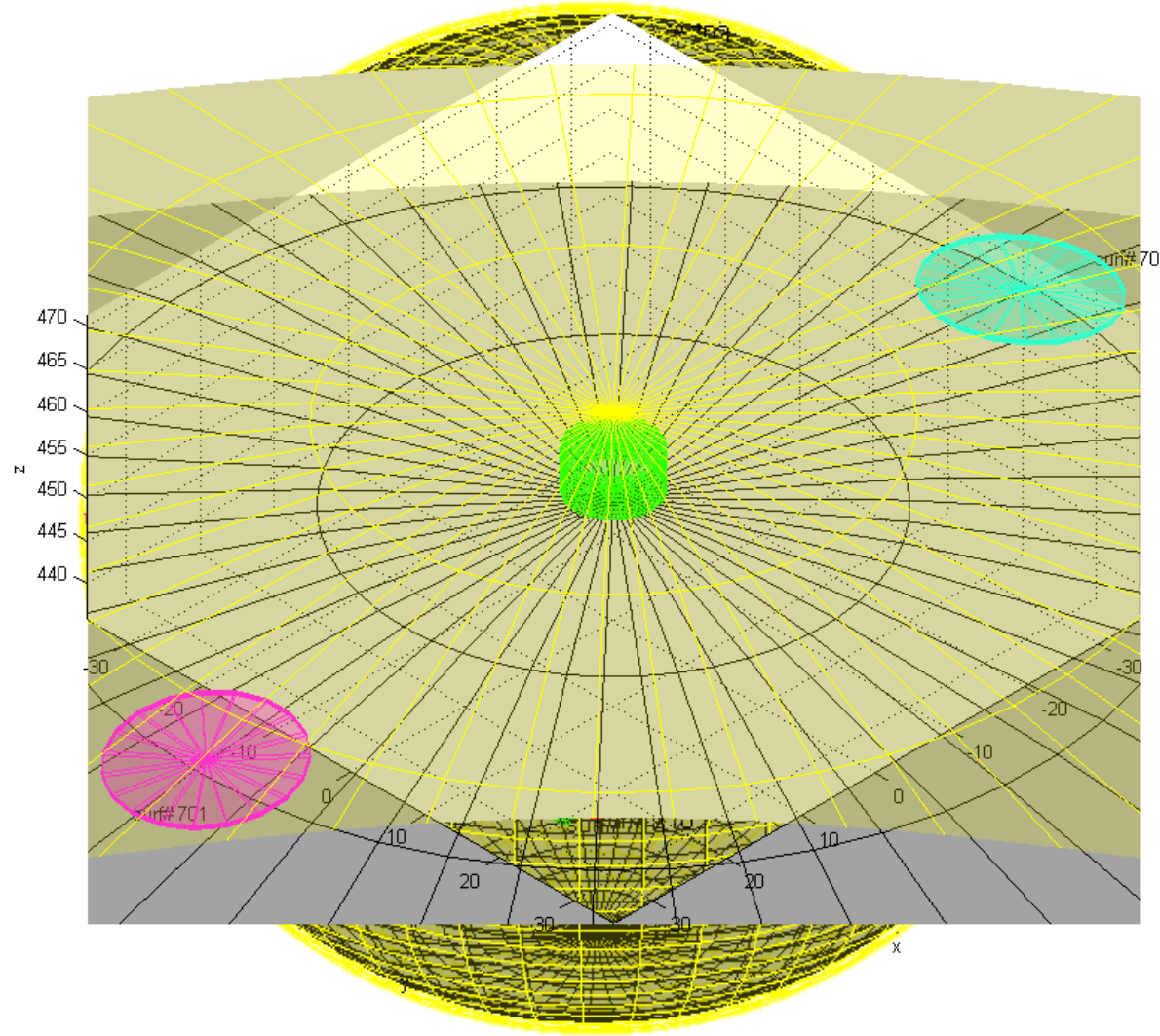
This work was performed under the auspices of the U.S. Department of Energy by Lawrence Livermore National Laboratory under Contract DE-AC52-07NA27344. Lawrence Livermore National Security, LLC



Sourced Neutron Energy Spectrum



ription



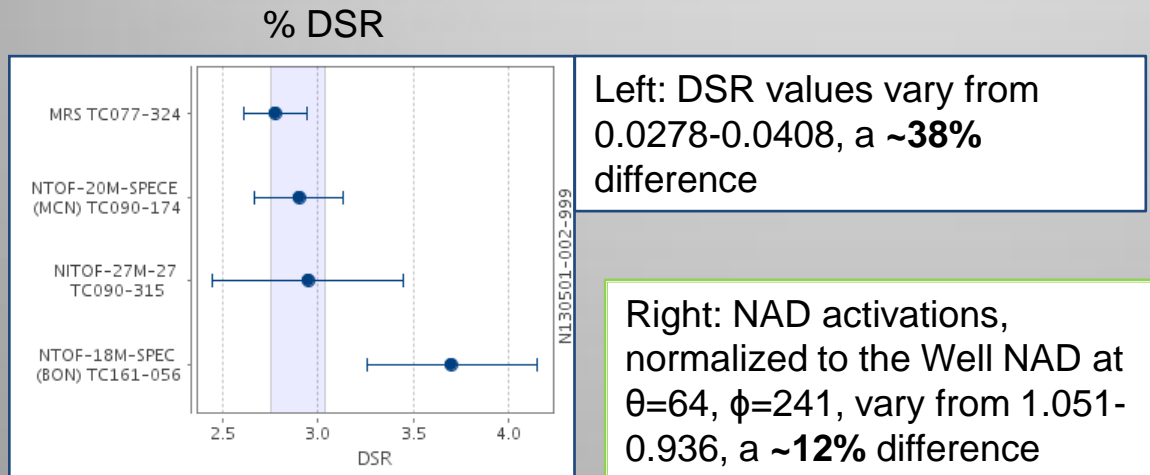
positions

Why is this Important?

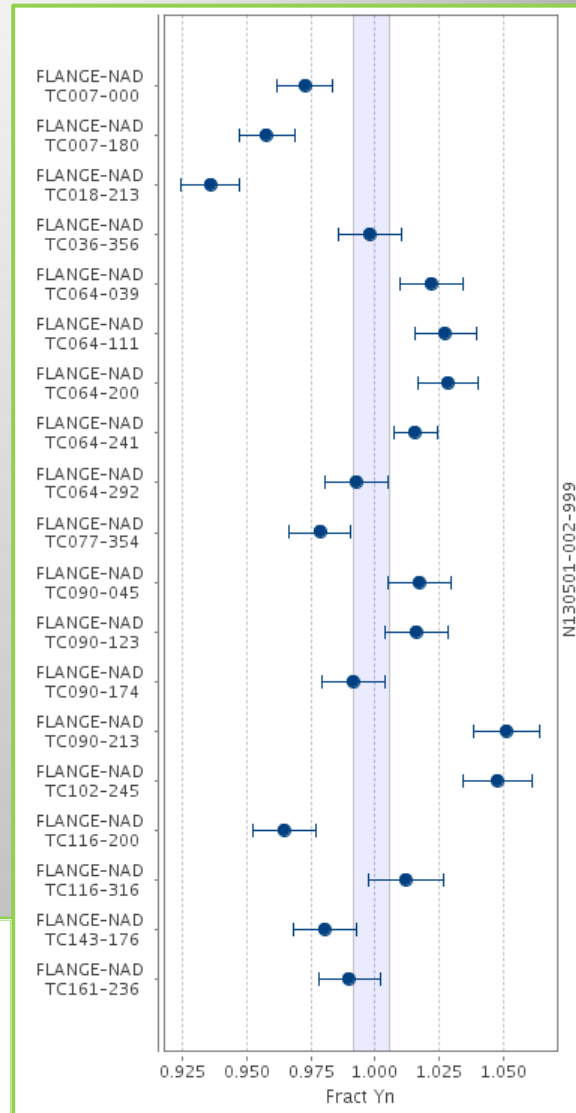
Recent NIF shots have seen significant asymmetries in the DSR and NAD activations.

If these measurements could be used to construct an image of the target geometry at bang time, this could be a significant asset in the effort to achieve ignition at NIF

Experimental results from the May 5, 2013 Highfoot Ablator DT NIF shot



Normalized NAD Activations



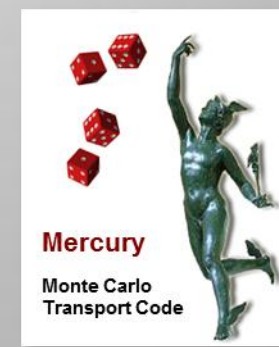
How can we model this?

Neutronics modeling was done using Mercury, a general purpose Monte Carlo particle transport code under development at LLNL

- Transports neutrons, photons, and light element (hydrogen and helium) charged particles
- Treats fixed source and criticality problems
- Written in C++ with a python user interface
- Runs efficiently on current generation massively parallel computing platforms

Define: “Monte Carlo”

A problem solving technique used to approximate the probability of certain outcomes by running multiple trial runs, called simulations, using random variables.



<http://www.investopedia.com/terms/m/montecarlosimulation.asp>

Project Goal:

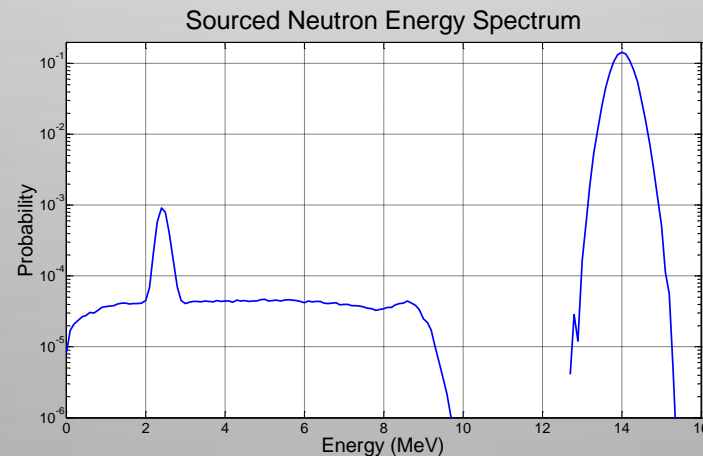
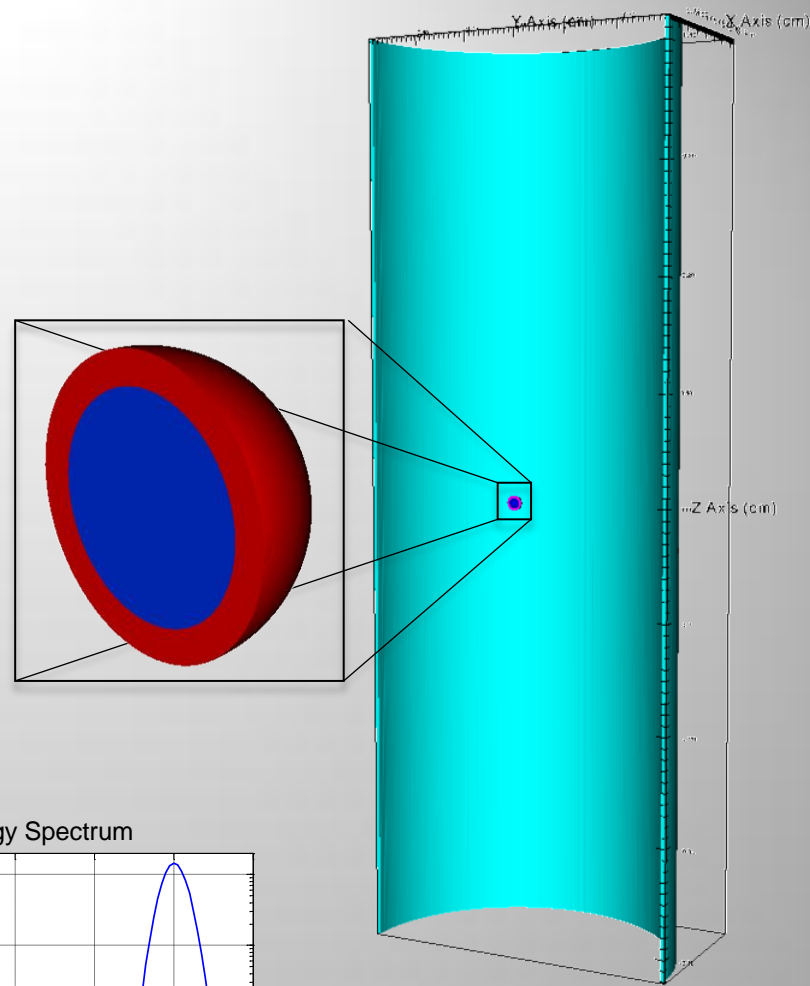
To take advantage of the ability of Mercury to

- describe complex geometries
- support different tallying (neutron counting) methods
- integrate easily with Python

in the modeling of complex 3D target systems

General Model

- Mass of DT ice shell held constant at **170 μ g**; mass of CH ablator (where modeled) held at **300 μ g**
- Point detectors to compute Zr activation and DSR placed on a 450cm radius sphere, at NAD and nTOF locations
- Gold activation via (n,2n) and (n, γ) reactions computed over the volume of the hohlraum
- Current tallies over the chamber surface and hotspot region surface
- Source spectrum describes the energy distribution of the fusion neutron, without thermalization effects



Hohlraum Dimensions

Inner radius	0.145 cm
Thickness	30 μ m
Length	0.84 cm

Outline

Mercury-MCNP

Benchmark spherically symmetric Mercury models of NIF target geometries against equivalent MCNP models:

- A point source, without an ablator
- A point source, including an ablator
- Compare surface flux tallies in both codes
- Check the relationship between computed DSR values and areal density (ρR) against published predictions

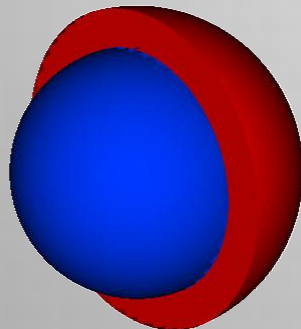
Mercury

Use Mercury to describe:

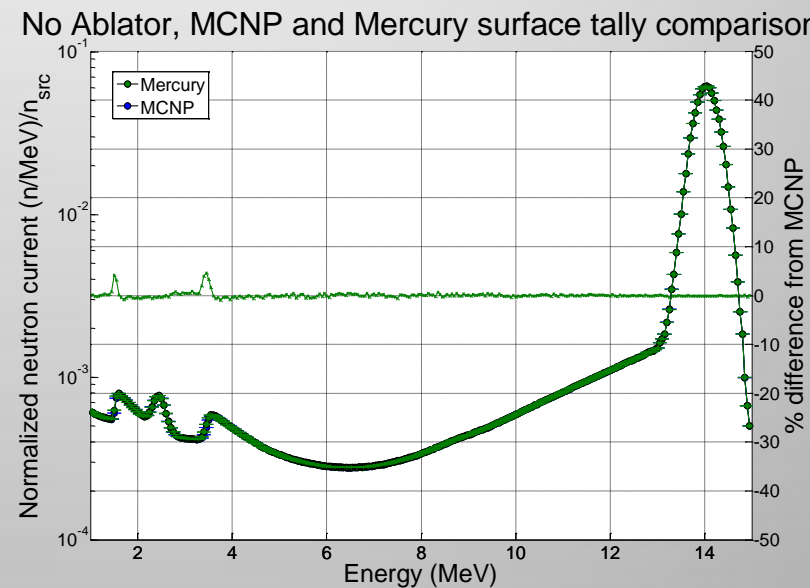
- A spherically symmetric case, with a distributed source
- A ‘teardrop’ shaped geometry, with the mass shifted towards the bottom
- Three different cases of sinusoidally varying thicknesses of the DT Ice layer
- Predict the $(n,2n)$ reactions in the Zr NADs, and the $(n,2n)$ and (n,γ) reactions in the gold hohlraum

We used spherically symmetric point source models to benchmark Mercury with MCNP

- Concentric Spherical Shells
- Point source at origin
- 50/50 DT gas region out to 38 um
- Dense 50/50 DT ice region, 38-48 microns



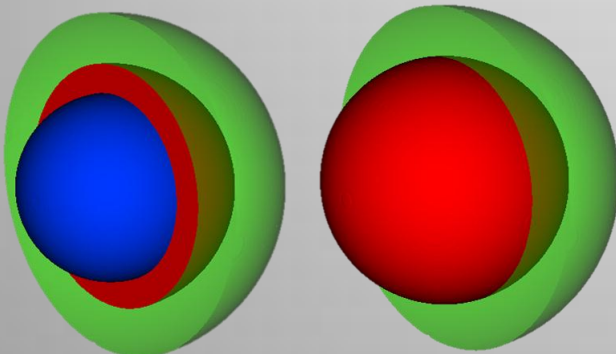
Region	Mass (μg)	Density (g/cm^3)	Thickness (μm)	ρR (g/cm^2)	T (keV)
DT Gas	7.67	33.4	38.0	0.127	3.5
DT Ice	170	600.0	11.7	0.700	0.15



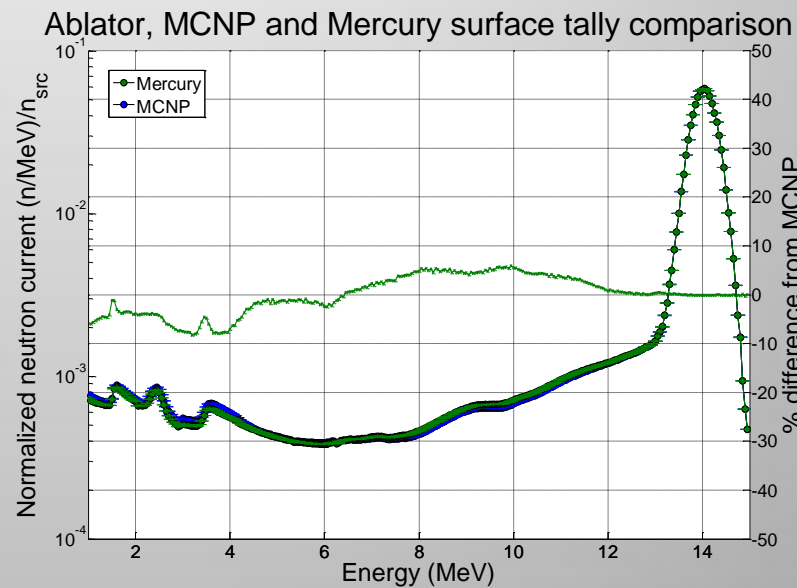
Mercury and MCNP spectra match for surface tallies at the chamber boundary

We investigated the impact of an ablator on both MCNP and Mercury models, using surface tallies

- Concentric Spherical Shells
- Point source at origin
- 50/50 DT gas region out to 38 microns
- Dense 50/50 DT ice region, 38-48 microns
- CH ablator, 48-68 microns

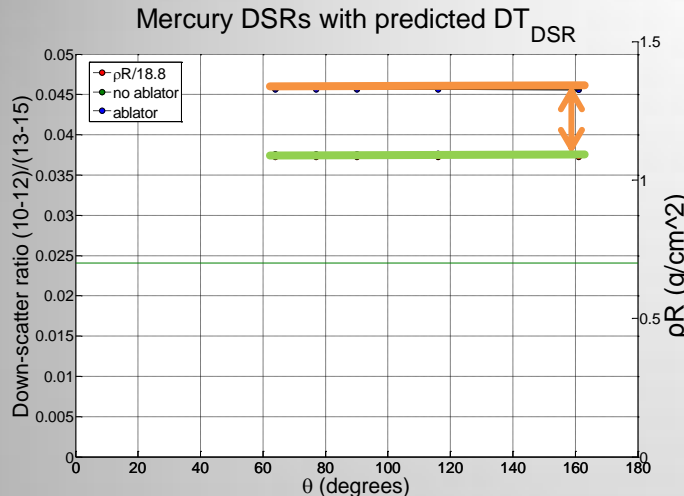


Region	Mass (μg)	Density (g/cm^3)	Thickness (μm)	ρR (g/cm^2)	T (keV)
DT Gas	7.67	33.4	38.0	0.127	3.5
DT Ice	170	600.0	11.7	0.700	0.15
CH Ablator	300	332.2	20.0	0.664	0.15



Mercury and MCNP spectra variation peaks at ~5% in the region of interest (10-15 MeV)

A 300 μg ablator has a significant effect on DSR



Model Description	DSR	σ	% diff	$\rho R/DSR$
ρR/18.8 (predicted)*	0.0372	~	~	18.8
MCNP, without ablator	0.0376	5.0E-06	0.87	18.6
Mercury, without ablator	0.0376	6.7E-06	0.98	18.6
MCNP, with ablator	0.0441	5.9E-06	18.53	15.9
Mercury, with ablator	0.0456	7.2E-06	22.54	15.3

For the case where
 $X = \rho R_{\text{ablator}} / \rho R_{\text{DT}} \sim 0.1$:

$$\rho R_{\text{tot}}(\text{g/cm}^2) = (20.4 \pm 0.6) \times dsr_{10-12\text{MeV}}$$

$$\rho R_{\text{fuel}}(\text{g/cm}^2) = (18.8 \pm 0.5) \times dsr_{10-12\text{MeV}}$$

Region	ρR (g/cm^2)
DT Gas	0.127
DT Ice	0.700
CH Ablator	0.664

* For our model, $X \sim 1$

Rev. Sci. Instrum. 83, 10D308 (2012); doi: 10.1063/1.4728095

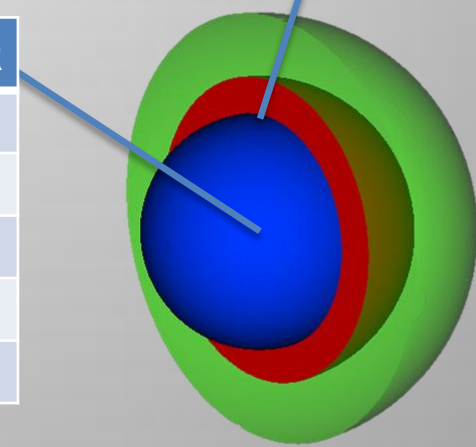
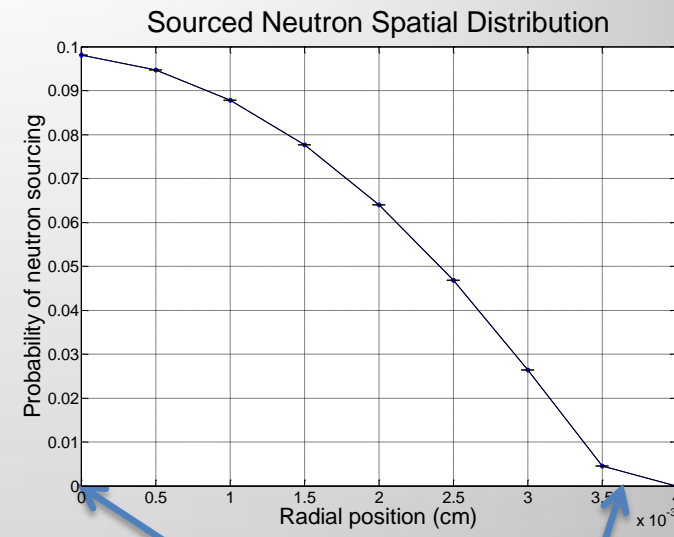
- DSR without the ablator matches Gatu Johnson predictions.
- DSR differences with ablator are understandable, since our modeled ablator ρR is $\sim 10x$ the Gatu Johnson value

We added a more realistic representation of the source spatial distribution

- Source is distributed over DT gas region; sourcing probability follows an inverted parabolic dependence on radius
- Geometry remained identical to spherically symmetric point-source model with ablator

Results:

Model Description	DSR	% diff	$\rho R_{DT}/DSR$
rhoR/18.8 (predicted)	0.0372	~	18.8
Point source, no ablator	0.0376	0.98	18.6
Distributed source, no ablator	0.0392	5.25	17.9
Point source, includes ablator	0.0456	22.5	15.3
Distributed source, includes ablator	0.0475	27.5	14.7



A distributed source affects the DSR measured through an ablator

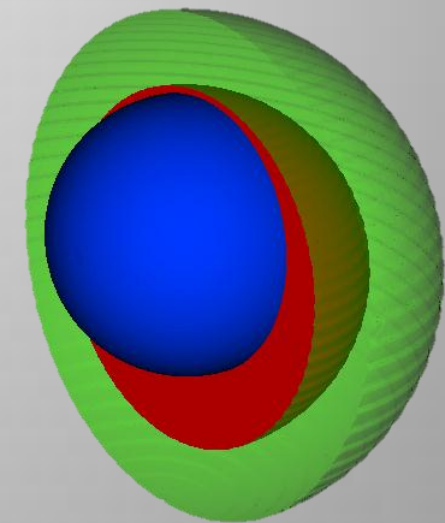
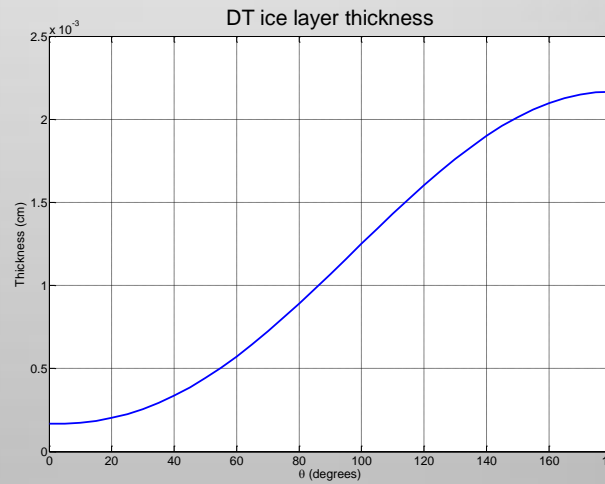
'Teardrop' model attempted to describe observed asymmetries

- Geometry meshed into 36 angular divisions of θ , each with constant properties
- 50/50 DT gas region out to 38 microns, contains distributed parabolic source
- Dense 50/50 DT ice region, beginning at 38 microns. ρR varies as

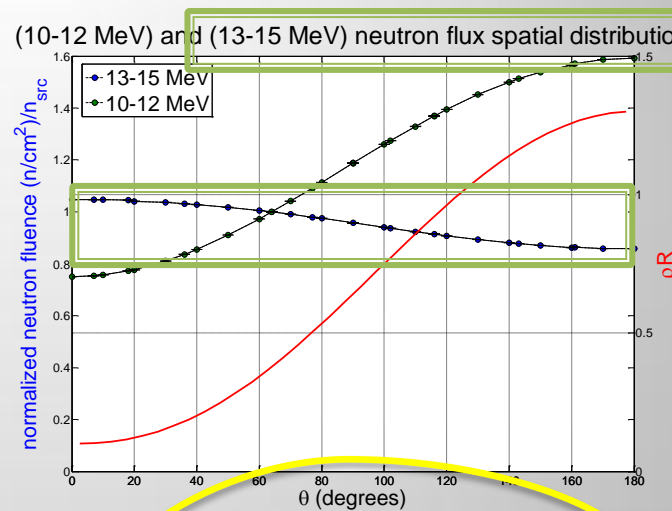
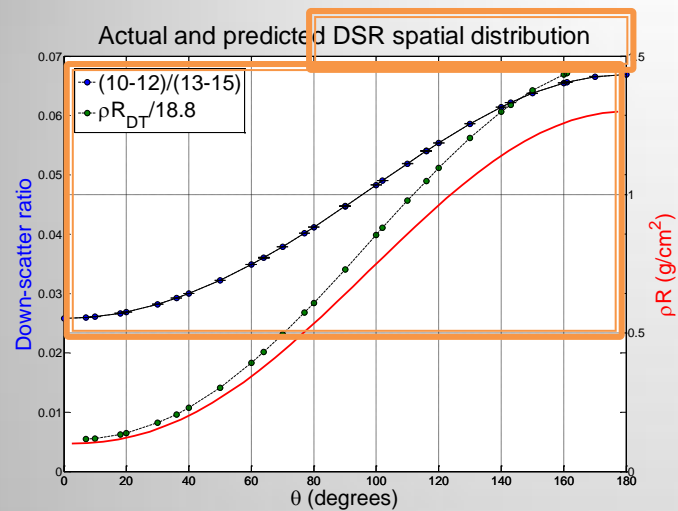
$$\rho R = 0.1 + 1.2 \cdot \sin(0.5 \cdot \theta)^{2.3}$$

- Constant ρR ablator (0.664 g/cm^2)

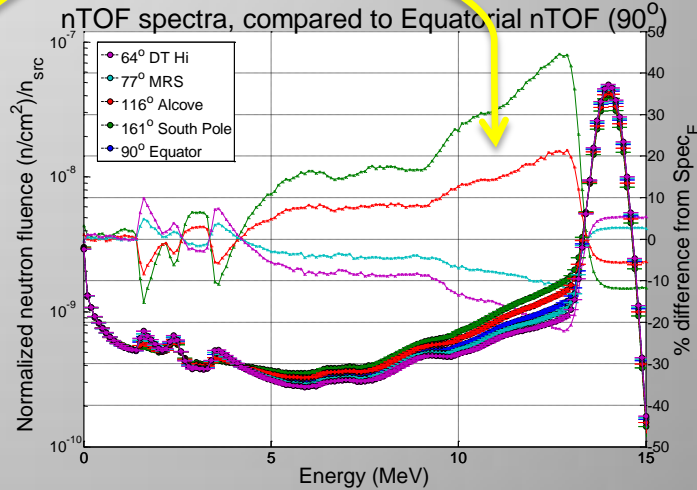
Region	Mass (ug)	Density (g/cm ³)	Thickness (um)	ρR (g/cm ²)	T (keV)
DT Gas	7.67	33.4	38.0	0.127	3.5
DT Ice	170	600.0	1.7 – 21.7	0.1 – 1.3	0.15
CH Ablator	300	332.2	20.0	0.664	0.15



'Teardrop' (0.5 θ) Model Results



nTOF	θ (degrees)	[10-12 MeV] flux	[13-15MeV] flux	DSR
DT_Hi	64	1.23E-08	3.42E-07	0.0361
MRS	77	1.34E-08	3.35E-07	0.0402
Equator	90	1.46E-08	3.27E-07	0.0447
Alcove	116	1.69E-08	3.12E-07	0.0540
South Pole	161	1.94E-08	2.95E-07	0.0656



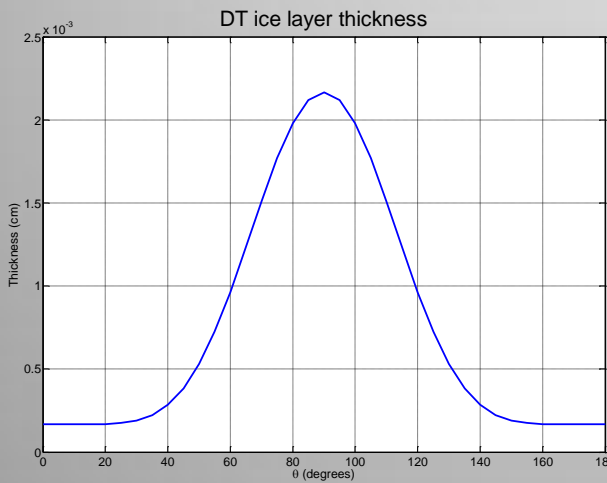
We observed a ~89% variation in the DSR (0.0258 - 0.0669), a ~20% variation in high (13-15 MeV) flux (0.86 - 1.05), and a ~72% variation in low (10-12 MeV) flux (0.75 - 1.60)

1 θ Model

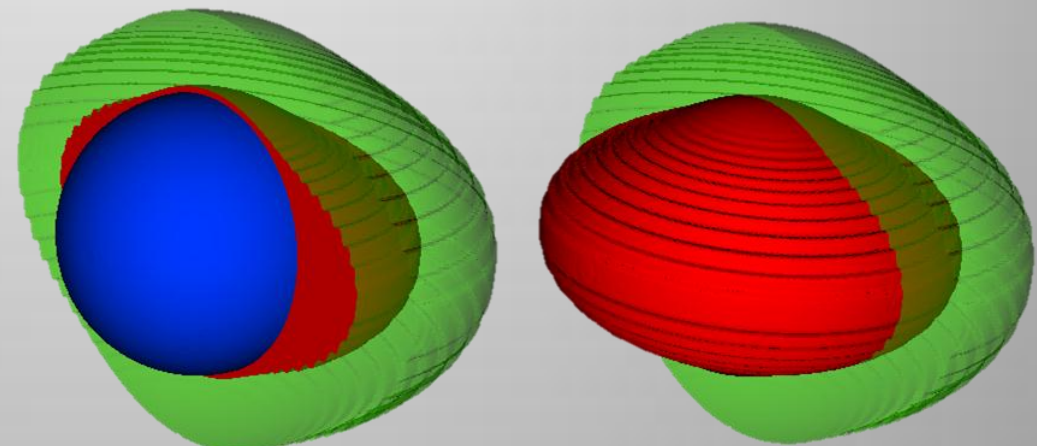
- Geometry of source and ablator same as 'Teardrop' model
- Dense 50/50 DT ice region, beginning at 38 microns. ρR varies as

$$\rho R = 0.1 + 1.2 * \sin(\theta)^{6.4}$$

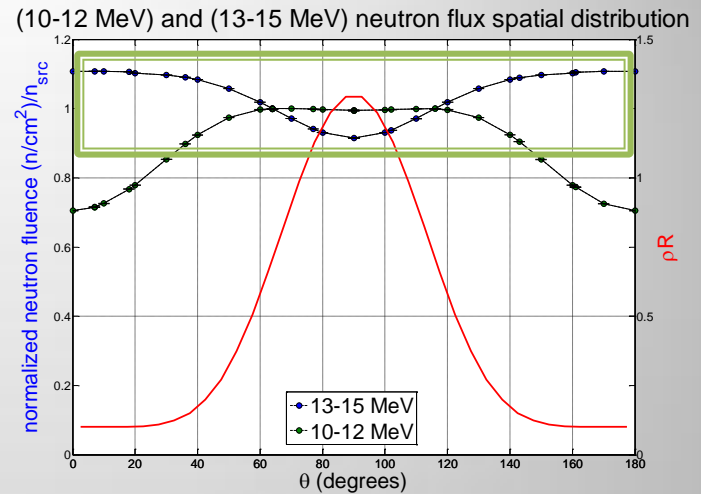
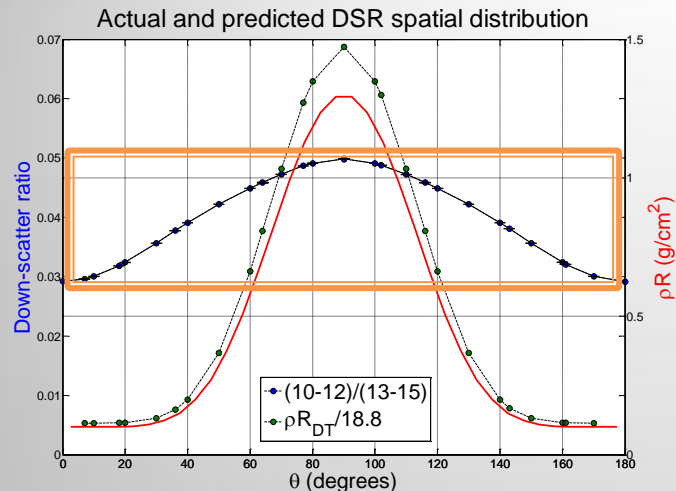
- Constant ρR ablator (0.678 g/cm²)



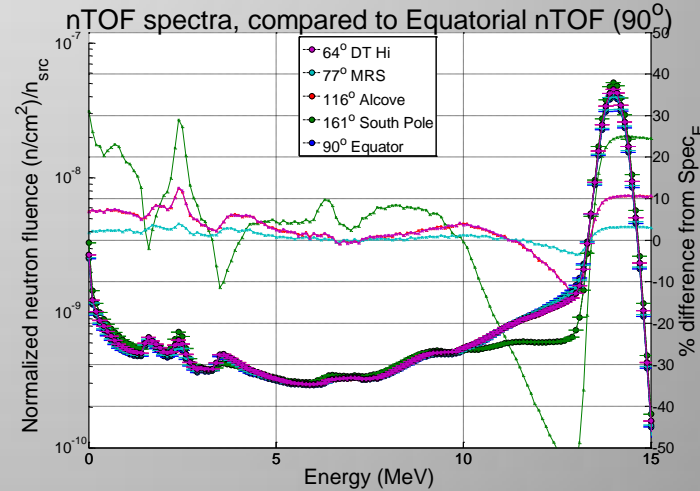
Region	Mass (ug)	Density (g/cm ³)	Thickness (um)	ρR (g/cm ²)	T (keV)
DT Gas	7.67	33.4	38.0	0.127	3.5
DT Ice	170	600.0	1.7 – 21.5	0.1 – 1.3	0.15
CH Ablator	300	339.2	20.0	0.678	0.15



1 θ Model Results



nTOF	θ (degrees)	[10-12 MeV] flux	[13-15MeV] flux	DSR
DT_Hi	64	1.49E-08	3.24E-07	0.0459
MRS	77	1.48E-08	3.04E-07	0.0487
Equator	90	1.48E-08	2.96E-07	0.0499
Alcove	116	1.48E-08	3.24E-07	0.0459
South Pole	161	1.15E-08	3.58E-07	0.0321



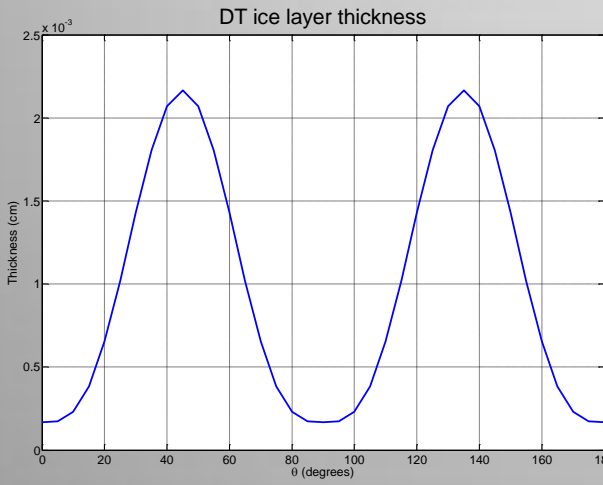
We observed a **~52% variation** in the DSR (0.029 - 0.050), a **~19% variation** in high [13-15 MeV] flux (0.92 - 1.11), and a **~34% variation** in low [10-12 MeV] flux (0.70 - 1.00)

2 θ Model

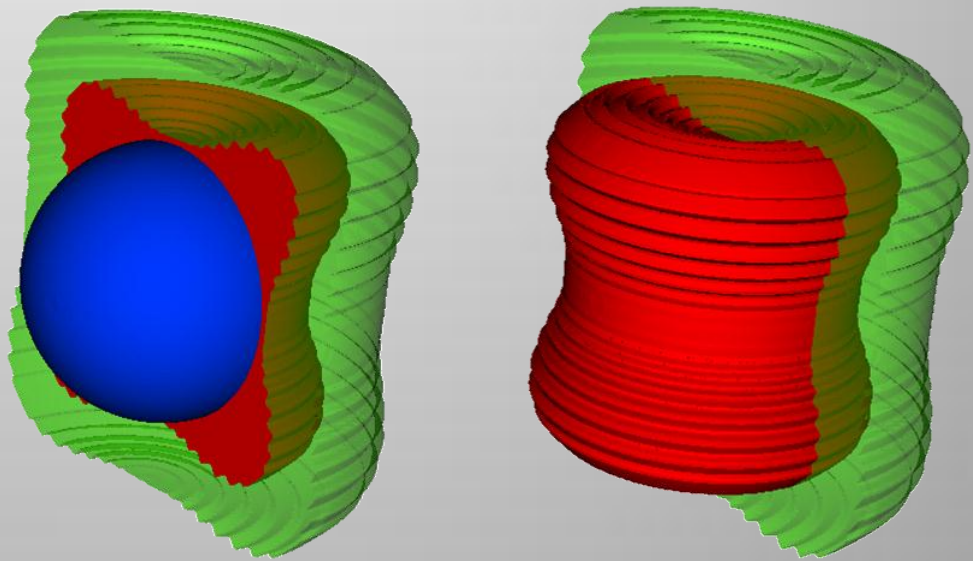
- Geometry of source and ablator same as 'Teardrop' model
- Dense 50/50 DT ice region, beginning at 38 microns. ρR varies as

$$\rho R = 0.1 + 1.2 * \sin(2 * \theta)^{3.2}$$

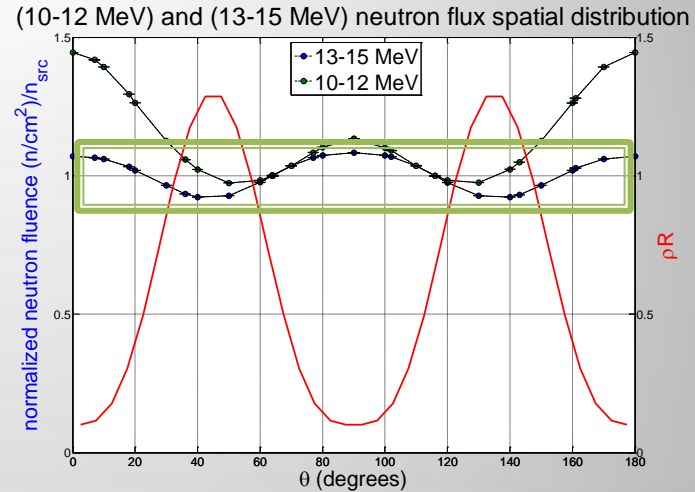
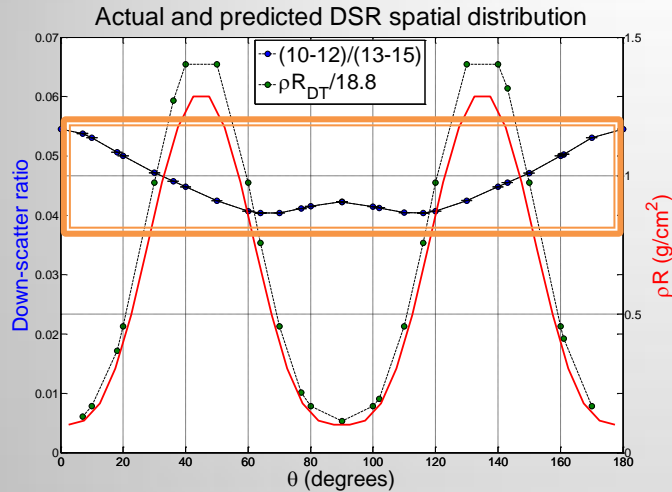
- Constant ρR ablator (0.678 g/cm^2)



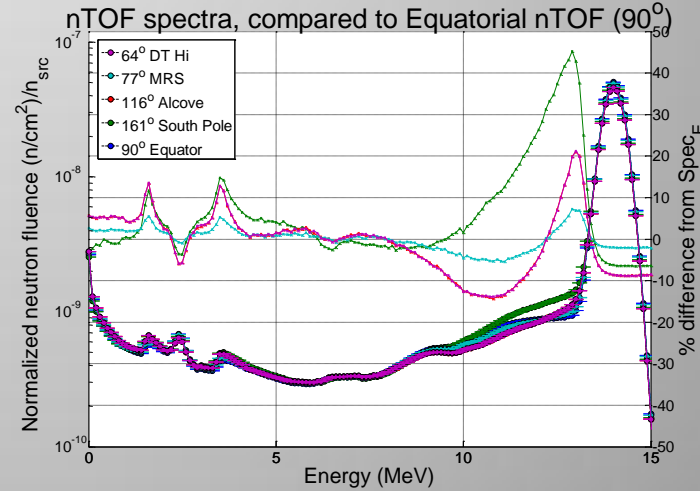
Region	Mass (ug)	Density (g/cm ³)	Thickness (um)	ρR (g/cm ²)	T (keV)
DT Gas	7.67	33.4	38.0	0.127	3.5
DT Ice	170	600.0	1.7 – 21.4	0.1 – 1.3	0.15
CH Ablator	300	339.2	20.0	0.678	0.15



2 θ Model Results



nTOF	θ (degrees)	[10-12 MeV] flux	[13-15MeV] flux	DSR
DT_Hi	64	1.32E-08	3.27E-07	0.0404
MRS	77	1.43E-08	3.48E-07	0.0411
Equator	90	1.50E-08	3.54E-07	0.0422
Alcove	116	1.32E-08	3.27E-07	0.0404
South Pole	161	1.69E-08	3.36E-07	0.0503



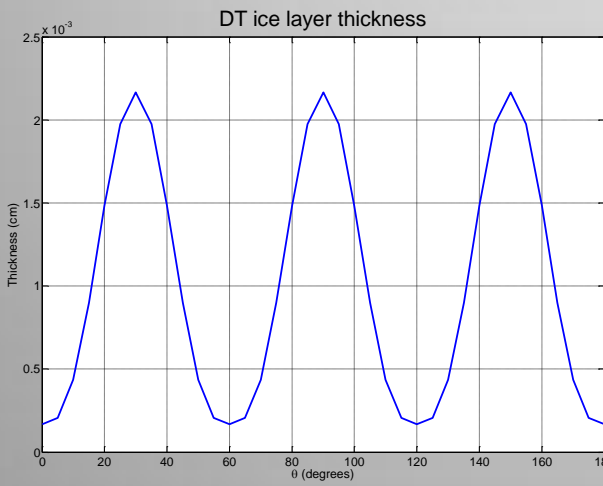
We observed a ~30% variation in the DSR (0.040-0.055), a ~16% variation in high [13-15 MeV] flux (0.92-1.08), and a ~39% variation in low [10-12 MeV] flux (0.97-1.44)

3 θ Model

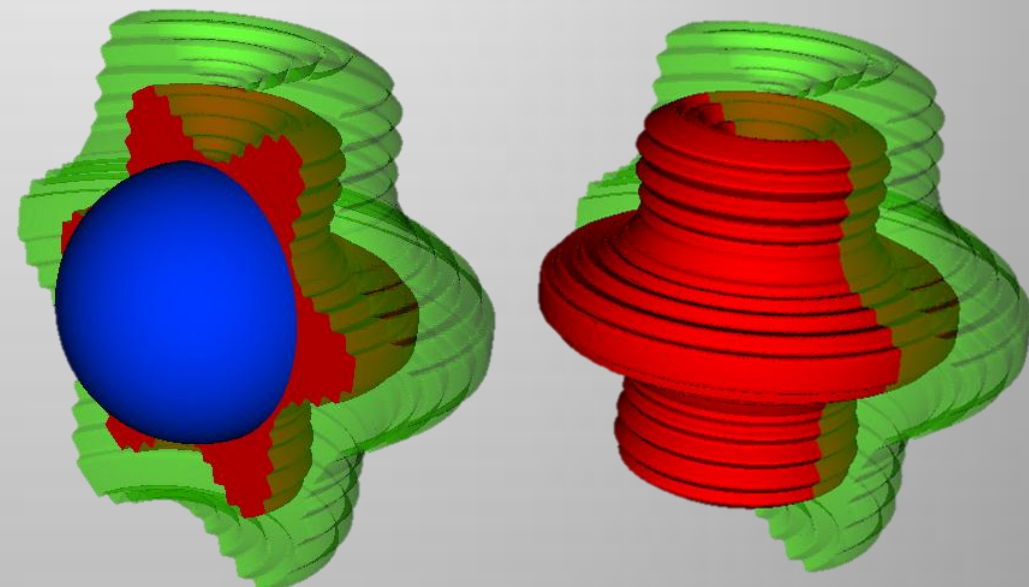
- Geometry of source and ablator same as 'Teardrop' model
- Dense 50/50 DT ice region, beginning at 38 microns. ρR varies as

$$\rho R = 0.1 + 1.2 * \sin(3 * \theta)^{2.9}$$

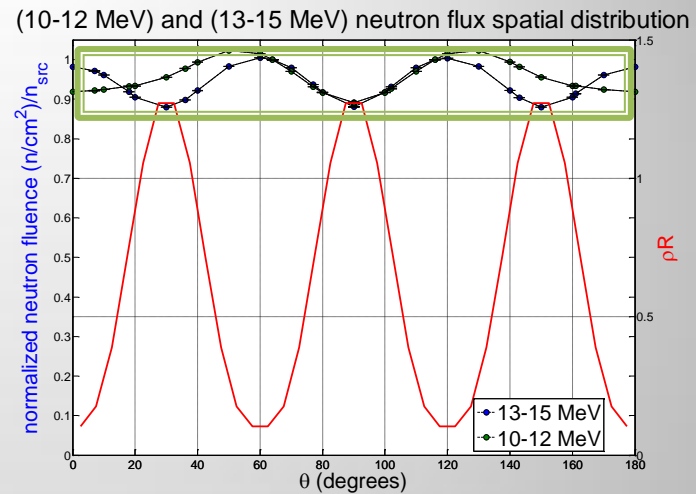
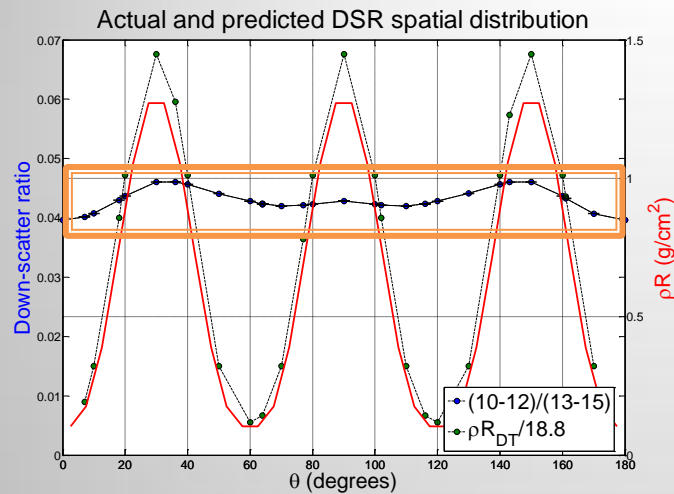
- Constant ρR ablator (0.678 g/cm²)



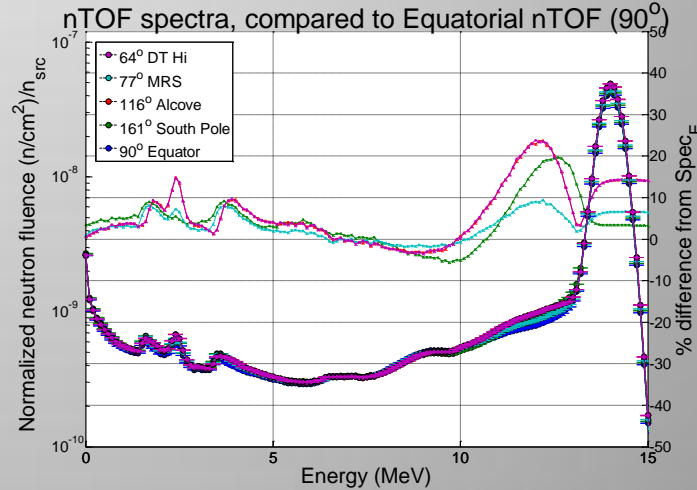
Region	Mass (ug)	Density (g/cm ³)	Thickness (um)	ρR (g/cm ²)	T (keV)
DT Gas	7.67	33.4	38.0	0.127	3.5
DT Ice	170	600.0	1.7 – 21.2	0.1 – 1.3	0.15
CH Ablator	300	339.2	20.0	0.678	0.15



3 θ Model Results

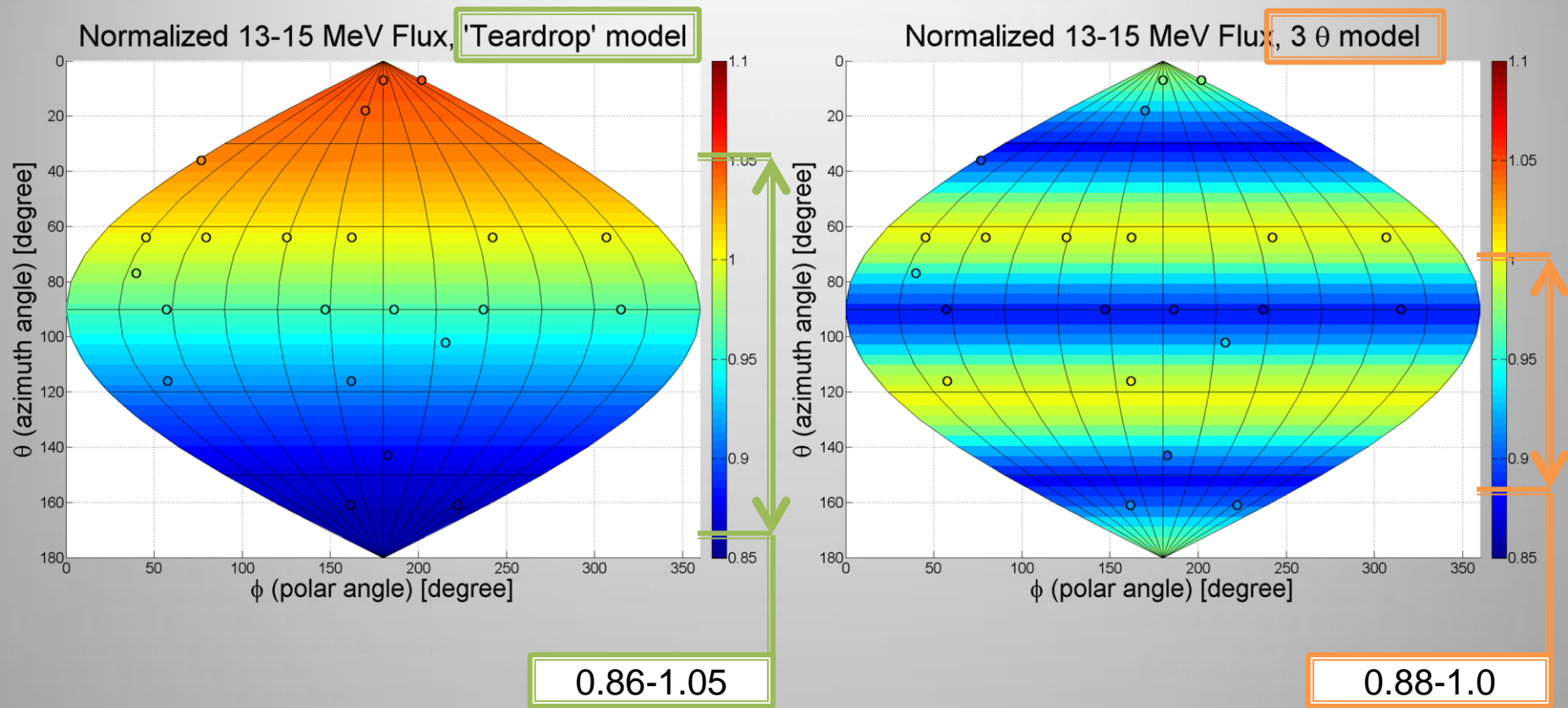


nTOF	θ (degrees)	[10-12 MeV] flux	[13-15MeV] flux	DSR
DT_Hi	64	1.47E-08	3.47E-07	0.0424
MRS	77	1.37E-08	3.26E-07	0.0421
Equator	90	1.31E-08	3.06E-07	0.0429
Alcove	116	1.47E-08	3.47E-07	0.0424
South Pole	161	1.37E-08	3.17E-07	0.0433

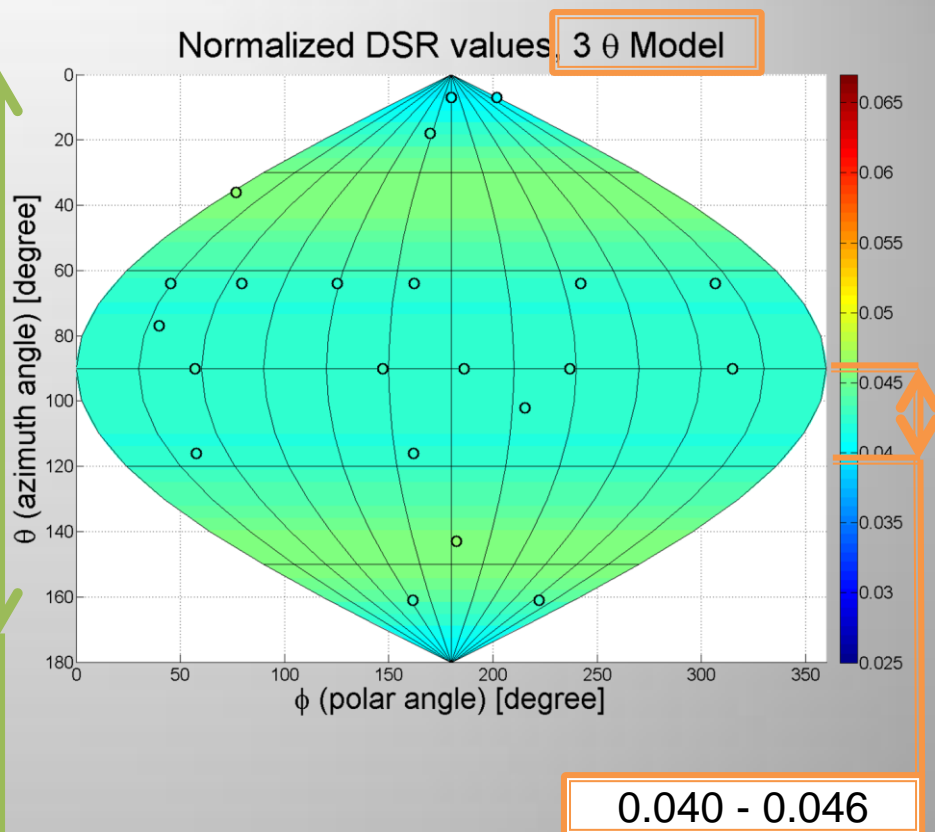
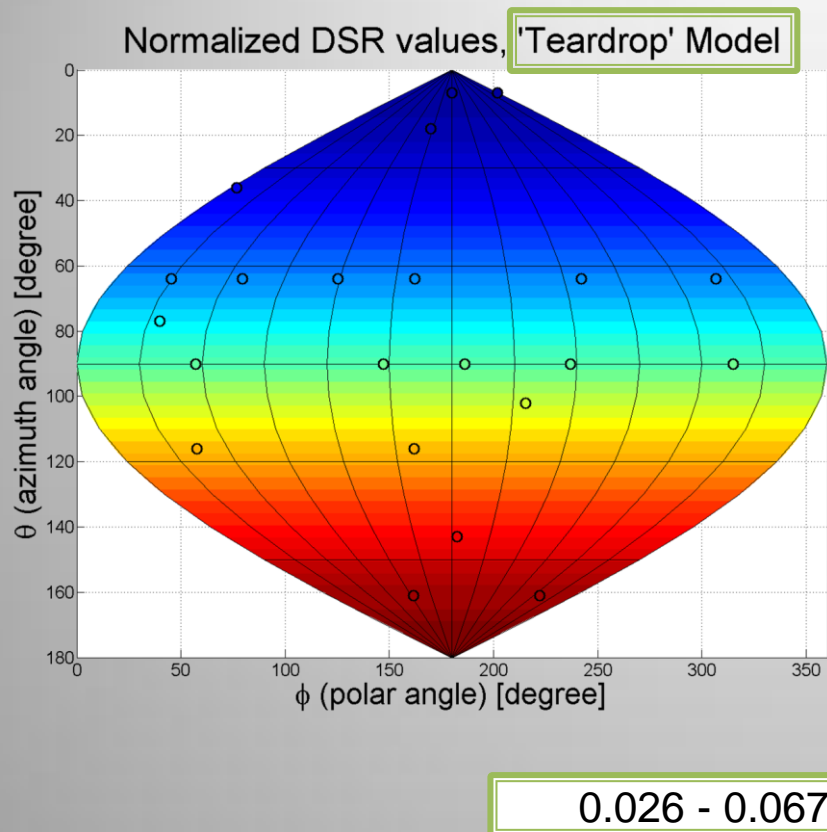


We observed a ~15% variation in the DSR (0.040-0.046), a ~13% variation in high [13-15 MeV] flux (0.88-1.00), and a ~14% variation in low [10-12 MeV] flux (0.89-1.02)

Measured (13-15 MeV) flux variation for a ρR range from [0.1-1.3] g/cm 2



Measured Down-Scatter Ratio variation for a pR range from [0.1-1.3] g/cm²



High mode structure appears to significantly suppress DSR asymmetries

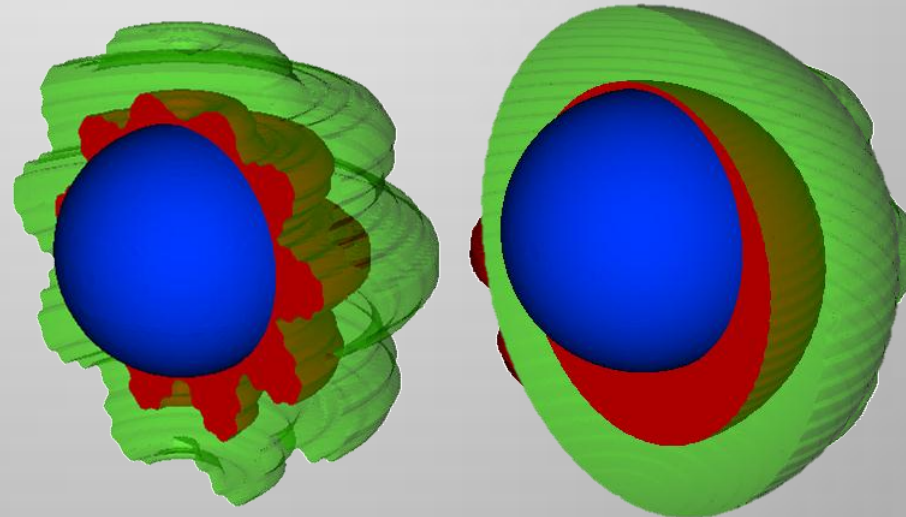
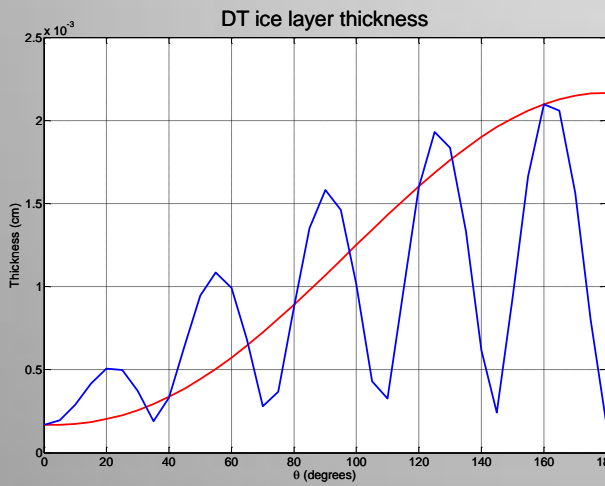
'Teardrop' * 5 θ Model

- Geometry of source and ablator same as 'Teardrop' model
- Dense 50/50 DT ice region, beginning at 38 microns. ρR varies as

Region	Mass (ug)	Density (g/cm^3)	Thickness (um)	ρR (g/cm^2)	T (keV)
DT Gas	7.67	33.4	38.0	0.127	3.5
DT Ice	170	600.0	2.1 – 21.5	0.1 – 1.3	0.15
CH Ablator	300	336.5	20.0	0.673	0.15

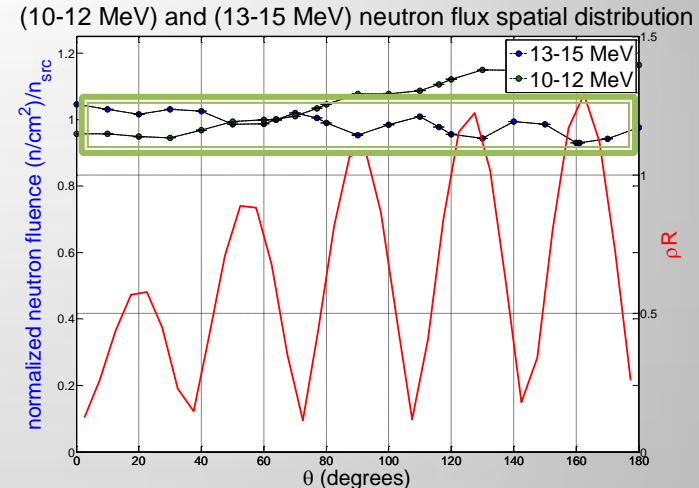
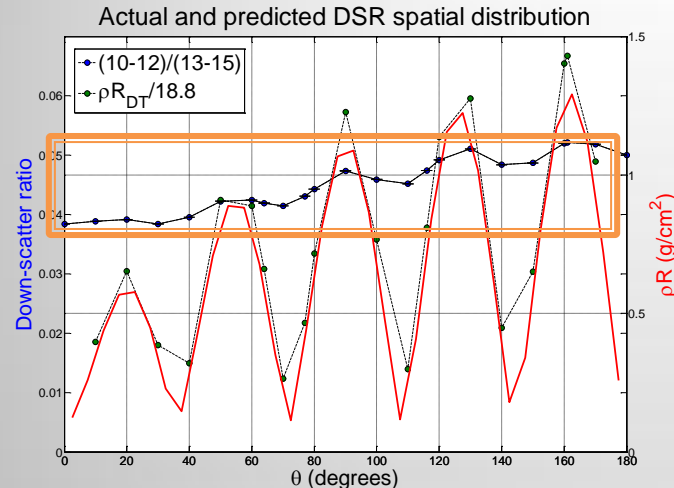
$$\rho R = 0.1 + 1.2 \sin(0.5 \theta) \sin(5 \theta)^{1.33}$$

- Constant ρR ablator (0.678 g/cm^2)

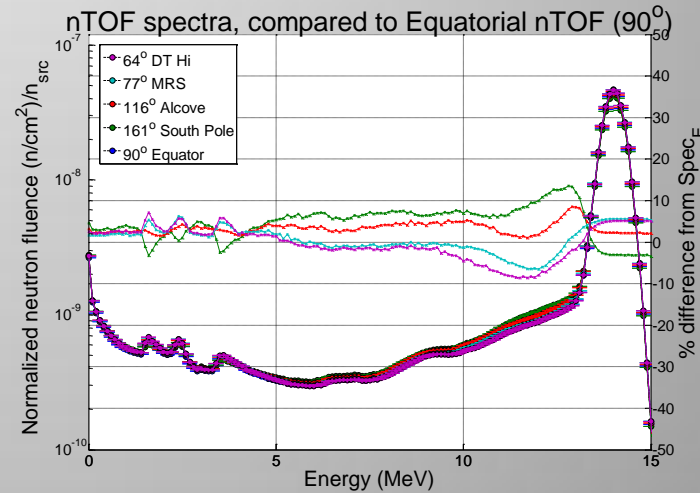


If high-mode structure 'washes out', this model should look similar to the 'Teardrop'

'Teardrop' * 5 θ Model Results



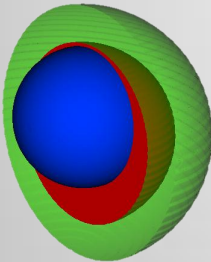
nTOF	θ (degrees)	[10-12 MeV] flux	[13-15MeV] flux	DSR
DT_Hi	64	1.39E-08	3.31E-07	0.0419
MRS	77	1.43E-08	3.33E-07	0.0431
Equator	90	1.50E-08	3.15E-07	0.0475
Alcove	116	1.53E-08	3.23E-07	0.0474
South Pole	161	1.60E-08	3.07E-07	0.0522



We observed a ~30.4% variation in the DSR (0.0384-0.0522), a ~11.8% variation in high [13-15 MeV] flux (0.93-1.05), and a ~20.8% variation in low [10-12 MeV] flux (0.95-1.17)

Compare – Teardrop/ Teardrop*0.5 θ

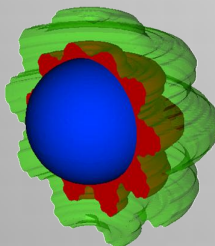
- Teardrop



nTOF	θ (degrees)	[10-12 MeV] flux	[13-15MeV] flux	DSR
DT_Hi	64	1.23E-08	3.42E-07	0.0361
MRS	77	1.34E-08	3.35E-07	0.0402
Equator	90	1.46E-08	3.27E-07	0.0447
Alcove	116	1.69E-08	3.12E-07	0.0540
South Pole	161	1.94E-08	2.95E-07	0.0656

~89% variation in the DSR (0.0258 - 0.0669), ~20% variation in high (13-15 MeV) flux (0.86 - 1.05), and ~72% variation in low (10-12 MeV) flux (0.75 - 1.60)

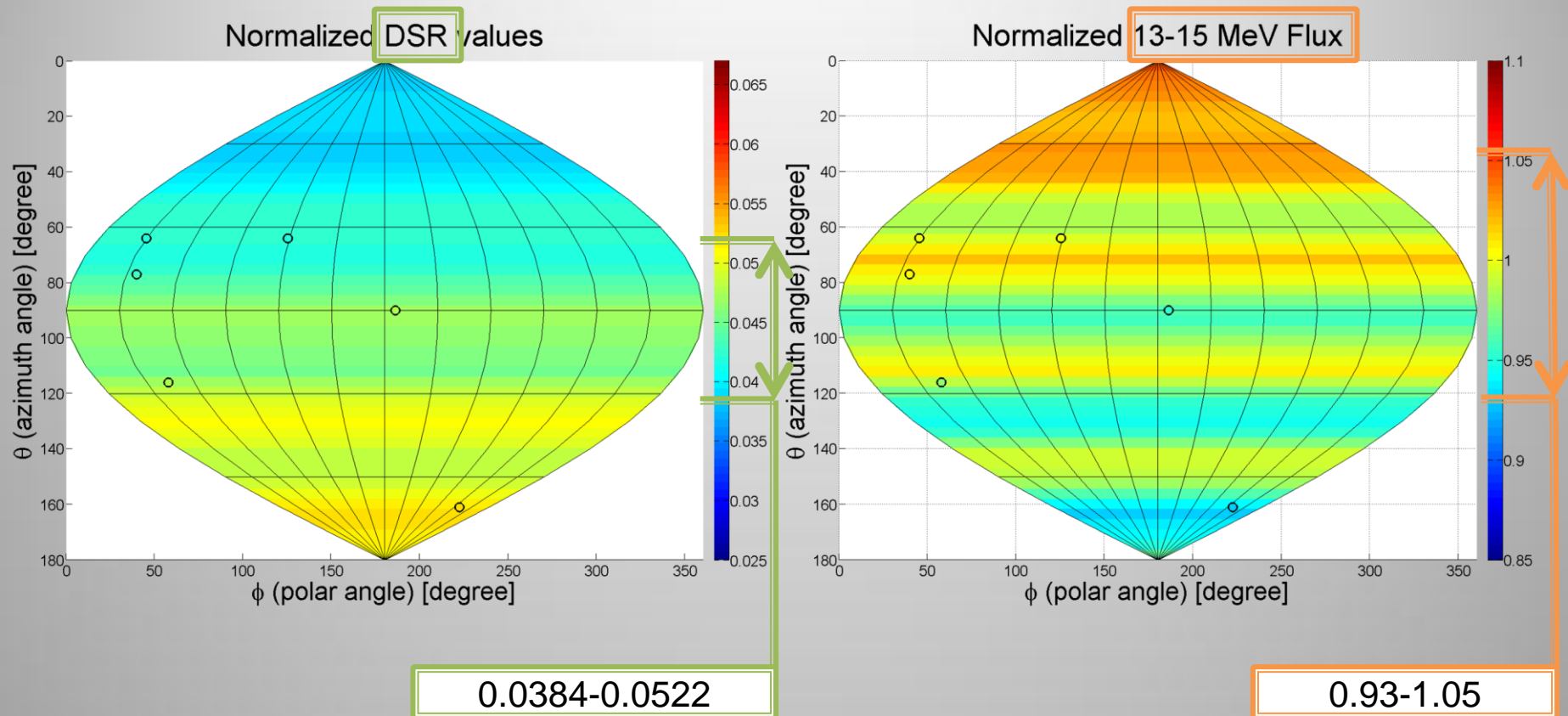
- Teardrop*0.5



nTOF	θ (degrees)	[10-12 MeV] flux	[13-15MeV] flux	DSR
DT_Hi	64	1.39E-08	3.31E-07	0.0419
MRS	77	1.43E-08	3.33E-07	0.0431
Equator	90	1.50E-08	3.15E-07	0.0475
Alcove	116	1.53E-08	3.23E-07	0.0474
South Pole	161	1.60E-08	3.07E-07	0.0522

~30% variation in the DSR (0.0384-0.0522), ~12% variation in high [13-15 MeV] flux (0.93-1.05), and a ~20.8% variation in low [10-12 MeV] flux (0.95-1.17)

Measured Down-Scatter Ratio variation for a pR range from [0.1-1.3] g/cm²

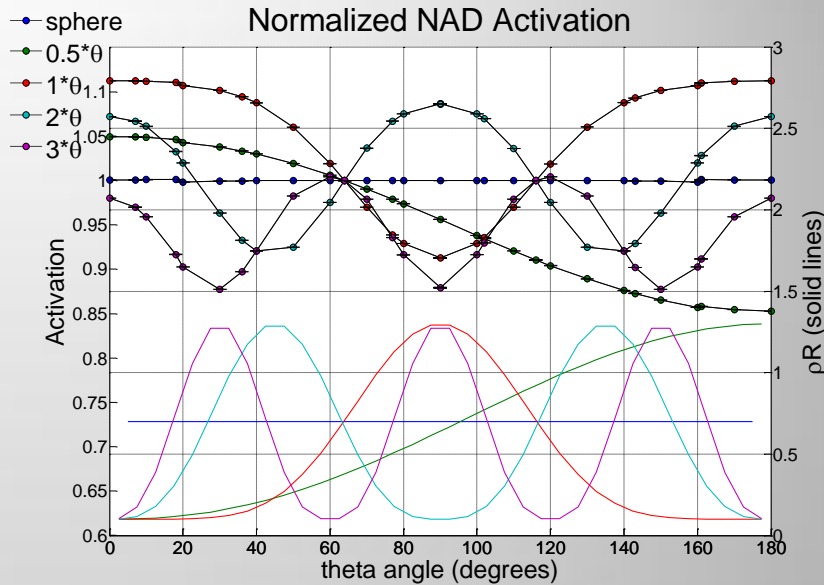


** Color ranges set to those used to span 'teardrop' data; DSR=[0.025 - 0.067] and flux=[0.85 - 1.1]

High mode structure in the 'Teardrop' suppresses observable asymmetries in high flux and DSR

Zirconium and Gold Activations

- Activation of materials can be computed in Mercury during problem execution.
- Zirconium at NAD positions (right)
- Gold over the hohlraum volume (below)



Gold (n,γ) and $(n,2n)$ reactions

Model	(n,γ)	$\sigma(n,\gamma)$	$(n,2n)$	$\sigma(n,2n)$	$(n,\gamma)/(n,2n)$	σ
sphere	0.002412	8.7E-06	0.1765	3.1E-06	0.01366	4.9E-05
0.5 θ	0.002423	9.1E-06	0.1773	3.0E-06	0.01366	4.9E-05
1 θ	0.002331	9.2E-06	0.1795	3.0E-06	0.01367	5.1E-05
2 θ	0.002218	7.9E-06	0.1760	3.0E-06	0.01299	5.1E-05
3 θ	0.002153	8.3E-06	0.1768	2.9E-06	0.01261	4.5E-05

Conclusions

Mercury-MCNP

- MCNP/Mercury calculations without ablator agree at high energies
- The effects of carbon scattering show differences

Mercury

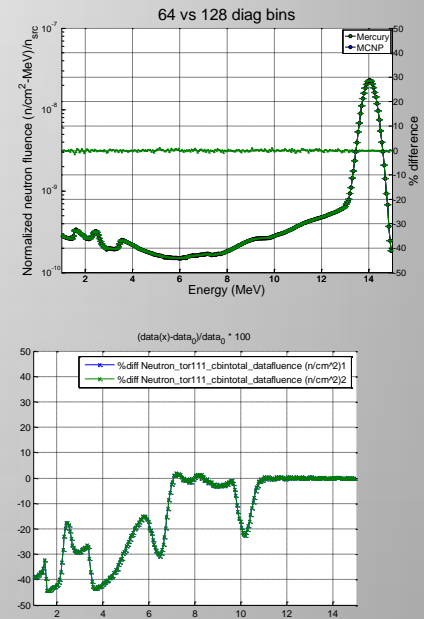
- 13-15 MeV flux (NAD activation) follows rhoR
- DSR variation decreases as target geometry becomes more complex

High mode structure appears to suppress fNAD and nTOF asymmetries

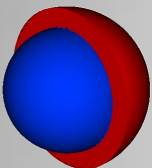
Special thanks to Andy Cook, to my mentors – Patrick Brantley, Charlie Cerjan, Scott McKinley, Scott Sepke – and to the Mercury team, especially Matt O'Brien and Ryan Bleile

Other

- No effect in changing ndiagbin to 128, with no ablator
- No effect in changing ndiagbin to 128, with ablator included
- No change in results between ‘meshed’ simple spherical case, and a simple spherical case made of concentric spheres.
- Standard deviations on Merc/MCNP are equivalent magnitude



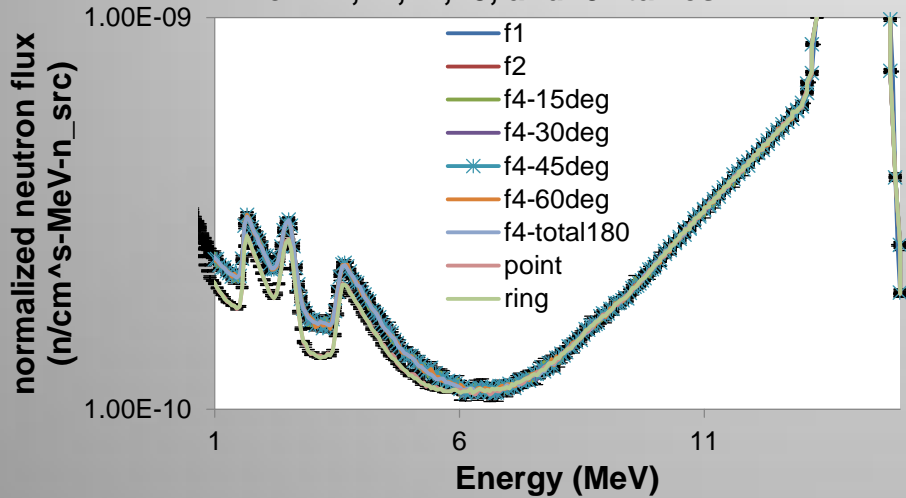
Unresolved difficulties were encountered while attempting to compare point detector fluences to flux tallied over the chamber boundary surface



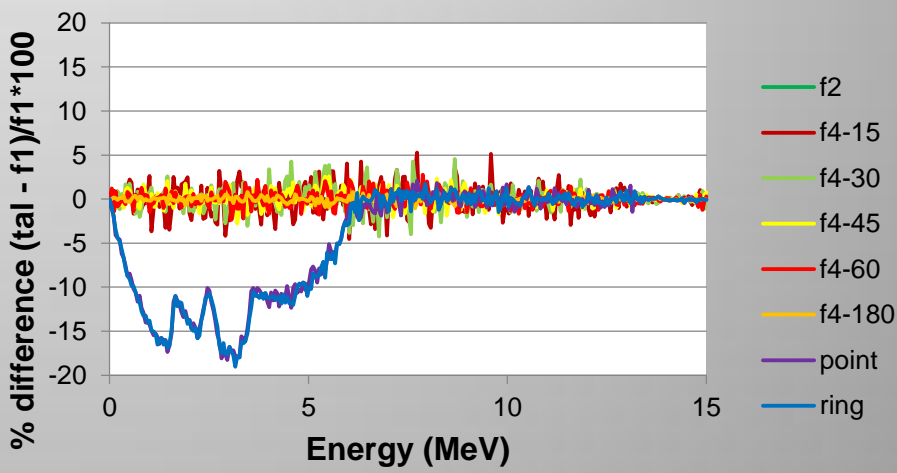
The differences observed between MCNP and mercury in point detector tallies prompted me to compare surface and point detectors within each code. MCNP's neutron fluence, when tallied at a point detector, do not appear to match with the same quantity tallied using a f1, f2, or f4 tally (current, surface, or volume tally)

MCNP Comparisons:

Neutron Flux/MeV at 450cm from origin- results from f1, f2, f4, f5, and f5z tallies



Percent differences from f1 tally, converted to units of flux



Although MCNP and Mercury point detector results do not match, Mercury diagnostic particle tallies do match transport particle tallies from both Mercury and MCNP, allowing them to be used